



Full Text View

[Volume 28, Issue 7 \(July 1998\)](#)

Journal of Physical Oceanography

Article: pp. 1346–1362 | [Abstract](#) | [PDF \(622K\)](#)

Separation of a Coastal Current at a Strait Level: Case of the Strait of Sicily

C. Herbaut, F. Codron, and M. Crépon

Laboratoire de Océanographie Dynamique et de Climatologie, Université Pierre et Marie Curie, Paris, France

(Manuscript received April 8, 1996, in final form July 25, 1997)

DOI: 10.1175/1520-0485(1998)028<1346:SOACCA>2.0.CO;2

ABSTRACT

The separation of a coastal current into two branches when encountering a strait, one entering the strait and the other crossing the strait and continuing to flow along the coast, is examined. Analytical solution shows that the strait topography plays a major role in the separation. When the depth of the sill of the strait is shallower than the ocean, double Kelvin waves propagate along the sill discontinuity line and are able to transport energy across the strait. The shallower the sill, the smaller the transport of the surface current entering the strait at the upstream corner and the larger the transport of the current transmitted across the strait. Sensitivity experiments done with a high-resolution primitive equation model confirm this behavior. These considerations explain the separation of the Algerian current into two branches at the Strait of Sicily: one entering the Eastern Mediterranean Sea and the other flowing into the Tyrrhenian Sea.

1. Introduction

The Western Mediterranean Sea is connected with the Atlantic Ocean by the Strait of Gibraltar and with the Eastern Mediterranean Sea by the Strait of Sicily. Both straits can be idealized as two-layer systems. In the Strait of Sicily the lighter surface Atlantic water flows into the Eastern Mediterranean Sea, while the Levantine Intermediate Water (LIW) enters the Western Mediterranean. The LIW inflow brings salty (38.7 psu) and warm (more than 14°C) water. The Atlantic water entering the Strait of Sicily originates from a separation of the eastward surface transport flowing in the Algerian Basin ([Béthoux 1980](#); [Millot 1987](#)). Observations show that two-thirds of the Atlantic water enters the strait of Sicily ([Béthoux 1980](#)) while one-third flows into the Tyrrhenian Sea ([Fig. 1](#)). The path of the Levantine Intermediate Water at the exit of the strait is more controversial. According to [Millot \(1987\)](#) and [Astraldi \(1995, personal communication\)](#), when leaving the Strait of Sicily, the LIW turns right along the Sicilian coast and follows a cyclonic path from the Strait of Sicily to the Strait of Gibraltar. However, according to [Manzella et al. \(1988\)](#), there is a

Table of Contents:

- [Introduction](#)
- [Flat bottom and sill](#)
- [Numerical experiments](#)
- [Conclusions](#)
- [REFERENCES](#)
- [TABLES](#)
- [FIGURES](#)

Options:


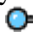
- [Create Reference](#)
- [Email this Article](#)
- [Add to MyArchive](#)
- [Search AMS Glossary](#)


Search CrossRef for:

- [Articles Citing This Article](#)

Search Google Scholar for:

- [C. Herbaut](#)
- [F. Codron](#)
- [M. Crépon](#)


The goal of this paper is to understand the mechanisms governing the separation of the surface water and the resulting circulation in the Strait of Sicily. In a previous paper ([Herbaut et al. 1996](#)), we investigated the response to the density gradient forcing through the Straits of Gibraltar and Sicily by numerical experiments. It appeared that the Atlantic inflow separates into two branches at the strait of Sicily level, one-half of the Atlantic water entering the strait and the other half flowing into the Tyrrhenian Sea ([Fig. 1a](#) ). The path of the Atlantic water is an important factor in the generation of the general cyclonic circulation of the Western Mediterranean. However, in the Herbaut et al. experiment, real topography and stratification were used. Therefore, the mechanism that induced the separation of the current at the entrance of the Strait of Sicily was not easy to understand. The topography of the region of the Strait of Sicily is characterized by a steep continental slope along the Algerian coast and a wide continental shelf west of the strait ([Fig. 1b](#) ). It is therefore difficult to identify which parameters are really important in driving the circulation.

In first approximation, the Algerian Current behaves as a boundary coastal jet ([Herbaut et al. 1996](#)). In the present study we therefore investigate the interaction of a coastal boundary current with a strait both by using analytical and numerical models. In the basic model, the geometry is represented by two flat bottom basins of different depths separated by a steplike topography, which represents the sill of the strait ([Fig. 2](#) ).

[Buchwald \(1968\)](#) showed that, in a homogeneous fluid, low-frequency Kelvin waves propagate around a right-angle corner without changing. In the high-frequency case however, cylindrical waves of the Poincaré type are generated at the corner and the amplitudes of the Kelvin waves are reduced. [Pinsent \(1971\)](#) studied the diffraction of a Kelvin wave propagating along a semi-infinite barrier when a depth discontinuity occurs at the edge of the barrier. As in Buchwald's study, Poincaré waves appear when the frequency of the incident wave is high, but double Kelvin waves can also exist if the frequency is low enough. These waves, first described by [Longuet-Higgins \(1968\)](#), are trapped along the depth discontinuity. [Gill et al. \(1986\)](#) examined the motion generated by a discontinuity of the surface elevation when the depth presents a step perpendicular to the surface elevation. Since the depth is different at each side of the step, the transport is also different and presents a discontinuity at the step generating double Kelvin waves propagating along it. For a stratified fluid, double Kelvin waves have both barotropic and baroclinic components. The adjustment is therefore more complicated. The generation by the wind of such waves along a submarine escarpment was studied by [Willmott \(1984\)](#). [Wajsowicz \(1991\)](#) investigated a problem similar to ours at the Iceland sill, but her numerical experiments were done with a resolution larger than the internal Rossby radius, which was not suitable to represent small-scale baroclinic flow.


This paper is structured as follows. In [section 2](#), we used a two-layer linear model in order to provide an analytical framework for understanding the behavior of a schematic case, that is, two flat bottom basins of different depths separated by a steplike topography. In [section 3](#), these analyses are compared with the results of a numerical simulation done with a linearized version of a 3D primitive equation model. First ([section 3b](#)), we studied the problem in the absence of topography (except for the sill), the coasts being represented by vertical walls. Since coastal topography modifies the structure of the initial wave front, the transport transmitted through the strait may be affected by this change. We therefore tested two types of topography. In [section 3c](#), we introduced a steep exponential bottom topography modeling the abrupt bathymetry off the coast of Algeria and examined its influence on the circulation. In [section 3d](#), the impact of a slowly varying shelf topography representing the bathymetry off Tunisia is tested. [Section 4](#) presents the conclusions.

2. Flat bottom and sill

The coastal current is generated by an incident Kelvin front as in [Speich et al. \(1996\)](#) and [Herbaut et al. \(1996\)](#). In the numerical experiments the initial density difference generating the incident Kelvin front is modeled by a horizontal alongshore density jump in the surface layer ([Fig. 2a](#) ) of the form $(\rho'_1 - \rho_1)Y(-x)$ at initial time [$Y(\cdot)$ being the Heaviside function].

Therefore, as the Fourier transform of $Y(\cdot)$ is $\delta(k) + (1/\pi)k$, the baroclinic Kelvin front is mostly composed of long and consequently low-frequency waves. The arrival of the incident baroclinic Kelvin front at the strait generates an adjustment. When there is no sill, the Kelvin front follows the coastline, turns right at the west strait corner, and penetrates into the strait without any change ([Buchwald 1968](#); [Crépon and Richez 1982](#)). When there is a sill however, the motion at the strait level is more complex. The interface displacement along the coast associated with the incident Kelvin front now generates two distinct motions: a baroclinic Kelvin wave front, which still penetrates inside the strait, and a double Kelvin wave propagating along the discontinuity line of the sill. In the linear case, the double Kelvin waves can be described analytically, and we can compute the transports associated with the currents inside the strait as function of the incident transport and the sill depth.

a. Equations

We consider a two-layer fluid located on a plane rotating around its vertical axis with a constant Coriolis parameter f . The variables in the top and bottom layers are designated by the subscripts 1 and 2 respectively. The general geometry is shown in [Fig. 2](#) . The top surface is considered as a rigid lid, and the mean depth H_1 of the top layer is constant, while the

bottom layer depth H_2 is variable (Fig. 2). The total depth $H = H_1 + H_2$. The interface height variation is given by h .

Further, we assume that the difference in density $\Delta\rho = \rho_2 - \rho_1$ is small compared to ρ_2 (Boussinesq's approximation) and note $\rho \approx \rho_1 \approx \rho_2$. We also neglect the nonlinear terms. The governing equations for the flow in each layer are (Allen 1975)

$$\partial_t u_1 - f v_1 = -\alpha \partial_x p_0 \quad (2.1)$$

$$\partial_t v_1 + f u_1 = -\alpha \partial_y p_0 \quad (2.2)$$

$$H_1(\partial_x u_1 + \partial_y v_1) - \partial_t h = 0 \quad (2.3)$$

$$\partial_t u_2 - f v_2 = -\alpha \partial_x p_0 - g' \partial_x h \quad (2.4)$$

$$\partial_t v_2 + f u_2 = -\alpha \partial_y p_0 - g' \partial_y h \quad (2.5)$$

$$\partial_x H_2 u_2 + \partial_y H_2 v_2 + \partial_t h = 0, \quad (2.6)$$

where $\alpha = 1/\rho$, $g' = g\Delta\rho$, and p_0 is the surface pressure.

Equations (2.3) and (2.6) are obtained by integrating the incompressibility equation from the bottom to the top of each layer. From these we derive a barotropic streamfunction, Ψ , which satisfies

$$H_1 u_1 + H_2 u_2 = -\Psi_y \quad \text{and} \quad H_1 v_1 + H_2 v_2 = \Psi_x.$$

Adding (2.1) and (2.4), (2.2), and (2.5) yields the governing equations for Ψ , which are of the form

$$\partial_t \Psi_y + f \Psi_x = \alpha H \partial_x p_0 + g' H_2 \partial_x h \quad (2.7)$$

$$\partial_t \Psi_x - f \Psi_y = -\alpha H \partial_y p_0 - g' H_2 \partial_y h. \quad (2.8)$$

Taking the curl of (2.7) and (2.8) yields

$$\partial_t \Delta \Psi = \mathbf{k} \cdot [\nabla H \times \nabla(\alpha p_0 + g'h)], \quad (2.9)$$

where $\Delta \Psi$ is the curl of the vertically integrated velocity and represents the barotropic component of the vorticity, and $\nabla(\alpha p_0 + g'h)$ is the gradient of the bottom pressure. The right-hand part of (2.9) identifies the JEBAR term.

We also define an equation for the evolution of the interface.

Subtracting (2.1) with (2.4) and (2.2) with (2.5) we determine an equation for \hat{u} and \hat{v} , where $\hat{u} = u_1 - u_2$:

$$\partial_t \hat{u} - f \hat{v} = g' \partial_x h \quad (2.10)$$

$$\partial_t \hat{v} + f \hat{u} = g' \partial_y h \quad (2.11)$$

$$\partial_x \hat{u} + \partial_y \hat{v} - \partial_t h \frac{H}{H_1 H_2} = \frac{1}{H_2} (u_2 \partial_x H_2 + v_2 \partial_y H_2). \quad (2.12)$$

The divergence and the curl of (2.10) and (2.11) with (2.12) yield the governing equation for the interface height h :

$$\partial_t \left(\Delta h - \frac{H}{g' H_1 H_2} (f^2 + \partial_t^2) h \right) = \frac{1}{g' H_2} (f^2 + \partial_t^2) \mathbf{u}_2 \cdot \nabla H, \quad (2.13)$$

which can be simplified for long-period motions ($\partial_t^2 \ll f^2$):

$$\partial_t \left(\Delta h - \frac{h}{r_2^2} \right) = \frac{f^2}{g'H_2} \mathbf{u}_2 \cdot \nabla H, \quad (2.14)$$

where

$$r_2 = \frac{1}{f} \sqrt{\frac{g'H_1 H_2}{H}}$$

is the Rossby radius of deformation for the first baroclinic mode.

We can also define the time evolution equations for the vorticity in each layer

$$\partial_t \left(\frac{\xi_1}{f} + \frac{h}{H_1} \right) = 0 \quad (2.15)$$


$$\partial_t \left(\frac{\xi_2}{f} - \frac{h}{H_2} \right) = \frac{1}{H_2} \mathbf{u}_2 \cdot \nabla H. \quad (2.16)$$

b. Adjustment at the arrival of the incident Kelvin front at the sill

The interface displacement associated with the incident Kelvin front generates a Kelvin front that propagates inside the strait along its western coast. There is thus a flow in the second layer crossing the sill at the western side of the strait. This flow and the associated bottom pressure constitute a forcing term for the barotropic streamfunction (2.9) and therefore generate a barotropic adjustment. Similarly a baroclinic adjustment is forced. In Eq. (2.16), the right-hand side term is a delta function and can only be compensated by a discontinuity of the vorticity in the second layer across the step because the interface elevation is continuous. As in the study of Gill et al. (1986), the discontinuity of the vorticity in the lower layer is due to the discontinuity of the along-step velocity. In the upper layer however, there is no discontinuity of the vorticity since the interface is continuous. These barotropic and baroclinic adjustments induce the propagation of double Kelvin waves before reaching a steady circulation. In the second layer, after the passage of the double Kelvin waves, there is no more flow crossing the sill. The flow crosses the sill only at the nose of the double Kelvin waves.

c. The double Kelvin waves

These waves are trapped near the escarpment and propagate with the shallower depth on the right (in the Northern Hemisphere; LeBlond and Mysak 1978). We study them in the two-layer rigid-lid case by dealing with long wavelengths as in Willmott (1984).

Consider a step topography such that the total depth H has two different values, H^+ for $y > 0$ and H^- for $y < 0$ where $H^+ > H^-$. The signs + and - will be used for all variables depending on y (Fig. 2 .

Let us assume all variables are of the form $\zeta(x, y, t) = \text{Re}[\zeta(x, y)e^{-i\omega t}]$.

When $\omega \ll f$ (low-frequency waves), Eqs. (2.9) and (2.14) become for $y \neq 0$

$$\Delta \Psi = 0 \quad (2.17)$$

and

$$\Delta h - \frac{h}{r_2^2} = 0, \quad (2.18)$$

where h and Ψ are functions of x and y only. The radius of deformation r_2 is different on each side of the step (denoted r_2^+ for $y > 0$ and r_2^- for $y < 0$).

Continuity at the step implies that the mass transport perpendicular to the step is continuous, which gives two conditions at $y = 0$: for the barotropic part

$$\Psi_x^+ = \Psi_x^- \quad (2.19)$$

and for the transport in the surface layer

$$\mathbf{v}_1^+ = \mathbf{v}_1^- \quad (2.20)$$

Continuity of the interface height h and of the surface pressure gradient $\partial_x p_0$ yields, using [\(2.1\)](#) and [\(2.20\)](#),

$$h^+ = h^- \quad (2.21)$$

and

$$u_1^+ = u_1^- \quad (2.22)$$

We seek solutions propagating along the escarpment of the form

$$\Psi = \Phi(y)e^{ikx} \quad (2.23)$$

and

$$h = H(y)e^{ikx}, \quad (2.24)$$

where $k > 0$.

By substituting [\(2.23\)](#) and [\(2.24\)](#) in [\(2.17\)](#) and [\(2.18\)](#) and solving the resulting system with the conditions [\(2.19\)](#) and [\(2.21\)](#) we obtain

$$\Psi = \Psi_0 e^{-k|y|} e^{ikx} \quad (2.25)$$

and

$$h = h_0 e^{-\lambda|y|} e^{ikx}, \quad (2.26)$$

where $\lambda^2 = k^2 + 1/r^2$.

Using [Eqs. \(2.10\)](#) and [\(2.11\)](#) and the expressions $Hu_1 = H_2 \hat{u} - \partial_y \Psi$ and $Hv_1 = H_2 \hat{v} + \partial_x \Psi$, we can compute the velocity components in the surface layer:

$$v_1^- = \frac{1}{H^-} \left[\frac{H_2^-}{f^2} (ig' \omega \lambda h_0 + ikfg'h_0) e^{-\lambda|y|} - ik\psi_0 e^{-\lambda|y|} \right] e^{ikx}$$

if $y < 0$.

With conditions (2.20) and (2.22) on the surface velocity, we obtain two relations between h_0 and Ψ_0 :

$$\Psi_0 + \frac{g'h_0}{f^2} \left[fH_1 - \frac{\omega H_2^- \lambda^- H^+ + H_2^- \lambda^+ H^-}{H^+ - H^-} \right] = 0$$

(2.27)

$$\Psi_0 + \frac{g'h_0}{f^2} \left[\omega H_1 \frac{H^+ - H^-}{H^- + H^+} - \frac{f H_2^- \lambda^- H^+ + H_2^- \lambda^+ H^-}{H^- + H^+} \right] = 0.$$

(2.28)

To have a solution not identically equal to zero, the determinant of these two equations must be zero. This leads to the dispersion relation for long waves:

$$\frac{\omega}{f} = \frac{H^- - H^+}{H^- + H^+}$$

$$\times \left[1 + \left(\frac{4H^+H^-}{H^+ + H^-} \right) \left(\frac{kH_1}{H_2^- \lambda^- H^+ + H_2^- \lambda^+ H^-} \right) \right].$$

(2.29)

For $k > 0$, ω/f has the same sign as $H^- - H^+$. The wave thus propagates with shallow depths on its right in the Northern Hemisphere. When k tends to zero, the phase speed increases to infinity. Moreover, according to (2.27) when k tends to 0, then h_0 also tends to 0. Therefore, these long waves are mostly barotropic.

In the present problem, we consider long waves (wavelengths of the order of the width of the strait). We make the approximation $kr_2 \ll 1$ since the strait width is much larger than r_2 . The velocity parallel to the step in the surface layer is then

$$u_1^+ = \frac{1}{H^+} \left(k\Psi - \frac{g'H_2^+ \lambda^+}{f} h \right), \quad y > 0 \quad (2.30)$$

$$u_1^- = -\frac{1}{H^-} \left(k\Psi - \frac{g'H_2^- \lambda^-}{f} h \right), \quad y < 0 \quad (2.31)$$

and in the deep layer

$$u_2^+ = \frac{1}{H^+} \left(k\Psi + \frac{g'H_1 \lambda^+}{f} h \right), \quad y > 0 \quad (2.32)$$

$$u_2^- = -\frac{1}{H^-} \left(k\Psi + \frac{g'H_1 \lambda^-}{f} h \right), \quad y < 0. \quad (2.33)$$

The velocities parallel to the step flow in opposite directions. Furthermore, u_1 is the sum of a barotropic component linked to Ψ and a baroclinic component linked to h . When kr_2 tends to 0, that is, when the wavelength is large compared to the internal radius of deformation, λ tends to $1/r_2$, and (2.29) becomes

$$\frac{\omega}{f} = \frac{H^- - H^+}{H^- + H^+}.$$

Substituting this value in (2.27) yields

$$k\Psi_0 = \frac{g'h_0}{f} \frac{H_2^+ \lambda^+ H^- + H_2^- \lambda^- H^+}{H^- + H^+}. \quad (2.34)$$

This shows that Ψ_0 and h_0 have the same sign. The barotropic and baroclinic components are thus opposed in the surface layer and added in the deep layer (Fig. 3 \Rightarrow).

Thus, according to (2.32) and (2.33) the zonal velocity in the second layer is discontinuous over the step. Moreover, the velocity has opposite signs on the two sides of the escarpment.

Let us now examine the total transport parallel to the escarpment in each layer. We find for $y > 0$,

$$\int_0^{+\infty} H_1 u_1 dy = \frac{H_1}{H^+} \Psi_0 - \frac{H_1 H_2^+}{H^+} \frac{g'}{f} h_0 \quad (2.35)$$

$$\int_0^{+\infty} H_2 u_2 dy = \frac{H_2^+}{H^+} \Psi_0 + \frac{H_1 H_2^+}{H^+} \frac{g'}{f} h_0. \quad (2.36)$$

For long waves and slow motions, relation (2.34) shows that the baroclinic terms of (2.35) and (2.36) (second term on the right side of these equations) are of order kr_2 and can thus be neglected with respect to the barotropic terms. The baroclinic component of the velocity is linked to interface elevation variations and consequently decreases quickly with respect to the distance from the escarpment [Eq. (2.24)]. This explains why it only contributes weakly to the total transport, even if it is important near the step. Its e -folding length scale is close to the baroclinic Rossby radii of deformation, whereas the e -folding length scale of the barotropic component is much larger since it is equal to the wavelength of the motion [Eq. (2.23)], which is the width of the strait at least in the present problem. It would be close to the barotropic Rossby radius in the free surface case for an infinite step. Therefore, far from the escarpment the flow is mostly barotropic.

d. Adjustment at the eastern corner of the strait

The double Kelvin waves propagate along the sill up to the eastern coast of the strait where a new adjustment occurs. There is no flow across the sill behind the double Kelvin front, but some flow can cross the sill at the nose of the wave front. In Gill et al. (1986), the double Kelvin front was due to the discontinuity of the cross-sill barotropic transport and propagated this discontinuity along the sill. In the present case, there is no discontinuity of the barotropic transport (because a rigid-lid model is used), but the transport in each layer is different at each side of the sill. The double Kelvin waves propagate this discontinuity in the transports. When the waves arrive at the eastern side of the strait, their propagation is stopped and the discontinuity in the transports generates the propagation of a baroclinic Kelvin front along the southern coast of the east–west basin. As it does at the nose of the double Kelvin front, the water of the lower layer located inside the strait crosses the sill at the eastern corner of the strait.

e. Transports

We can estimate the amplitudes of these motions and the associated transport by considering the mass continuity. From (2.33) and (2.34) one can see that the mass transport associated with the baroclinic motion is $r_2^2 f h$, where h is the amplitude of the interface elevation at the coast (or above the sill). The barotropic transport is $(H_1/H)\Psi_0$ in the surface layer and $(H_2/H)\Psi_0$ in the deep one. Let us now define h_i as the amplitude of the interface elevation of the incident Kelvin wave, h_d the amplitude of the interface elevation along the step, and h_s the amplitude of the Kelvin wave propagating inside the strait. Mass continuity in the deep layer along the $y = 0$ coast and the no-flow condition across the sill then give

$$H_1 \frac{g'}{f} (h_i - h_d) = \Psi_0 \quad \text{and} \quad H_1 \frac{g'}{f} (h_s - h_d) = \Psi_0,$$

which yields $h_i = h_s$.

It results that the interface elevations of the incident motion and the motion along the western coast of the strait have the same amplitude.

Similarly, the transport continuity at $x = B$ (B being the width of the strait) gives

$$h_r = h_i \left(1 - \frac{H^- H_2^+}{H^+ H_2^-} \right),$$

where h_r is the amplitude of the “transmitted” baroclinic motion flowing along the part of the south coast located east of the strait.

The transport associated with the baroclinic motion flowing along the western coast of the strait is, therefore,

$$T_s = \left(\frac{r_2^-}{r_2^+} \right) T_i = \frac{H_2^- H^+}{H_2^+ H^-} T_i \quad (2.37)$$


and that of the transmitted baroclinic motion is

$$T_r = T_i - T_s. \quad (2.38)$$

The barotropic transport in the gyre can be estimated by neglecting the baroclinic component of the double Kelvin wave. We then find

$$\Psi_0 = \frac{H^-}{H_2^-} T_i,$$

where T_i is the transport in any layer in the incident wave.

In summary, the circulation obtained is first composed of a baroclinic current generated by the incident baroclinic front flowing along the western part (west of the strait) of the southern coast of the basin. At the western corner of the strait, the surface flow divides in two branches. One branch enters the strait and follows the western coast of the strait (this flow is associated with a baroclinic Kelvin front). The second branch flows along the step discontinuity (the current is associated with the double Kelvin waves) and then along the eastern part (east of the strait) of the southern coast of the basin. In the second layer, the incident current, which is directed westward, does not enter the strait but is trapped by the escarpment and flows along it. This westward current is fed at the eastern corner of the strait by a current flowing out of the strait and by a westward current flowing along the southern coast of the basin east of the strait (this latter current is generated by the Kelvin front, which propagates east of the strait). The transports of these currents depend on the ratio of the baroclinic Rossby radius, that is, on the ratio of the depth on both parts of the step: the shallower the sill, the smaller the transport of the surface current entering the strait at the western corner and the higher the current transmitted across the strait (Fig. 4 )

3. Numerical experiments

a. Model description

The basic geometry represents an idealized strait. It is composed of a deep basin where the south zonal coast is crossed by a shallow strait. The total depth is 1000 m in the basin, and 500 m in the strait. The width of the strait is 130 km, which is much larger than the internal radius of deformation, which is about 14.7 km. The total length of the basin is 650 km and its width is 500 km.

The fluid is composed of a layer of constant density 850 m deep and a surface layer of lighter density 150 m deep (Fig. 2

•). The reduced density between the two layers is $\Delta\rho = 1.3 \times 10^{-3}$, giving a Rossby radius for the first baroclinic mode of 14.7 km (at 38°N). In the western part of the basin, at $x = -L$, there is a north–south gate separating an area where the density of the surface layer is lower than in the eastern part. This horizontal density gradient is only used to generate the Kelvin front by pressure difference but is not advected in the linear model. The intensity of the coastal current depends on this horizontal density gradient, whereas the spatial structure of the current is related to two-layer vertical structure.

Numerical experiments were performed with the 3D primitive equation model OPA7 of the LODYC (Andrich et al. 1988; Madec et al. 1991a,b). The model is a level model with a rigid lid filtering barotropic gravity waves. The horizontal discretization on an Arakawa C grid uses a tensorial formalism, which allows a second-order accuracy scheme on any orthogonal three-dimensional curvilinear mesh. In this study, the vertical coordinate is a z coordinate and the pressure is hydrostatic. A detailed description of the model equations is given in Madec et al. (1991a), and we briefly present here the main characteristics used in the simulations. Subgrid-scale physics is parameterized by a fourth-order operator for momentum and tracers. The horizontal eddy viscosity and diffusion coefficients are equal to $-10^{+9} \text{ m}^4 \text{ s}^{-1}$ (as we use a bi-Laplacian) and the vertical coefficients are assumed to vary as a function of the local Richardson number according to the parameterization proposed by Pacanowski and Philander (1981). They range from the molecular viscosity to a maximum value of $10^{-2} \text{ m}^2 \text{ s}^{-1}$ when the Richardson number is zero. The horizontal grid has a 5-km resolution, that is, one-third of the deformation radius, and we use 25 vertical levels with a gap of 25 m near the surface and the interface, increasing deeper until reaching 140 m at the bottom. The time step is 10 min, allowing the propagation of waves with phase speeds of 8 m s^{-1} , whereas baroclinic Kelvin waves theoretically propagate at only 1.4 m s^{-1} .

Two “sponge layers” were implemented in the southern part of the strait in order to simulate its opening into a second basin and into the eastern part of the main basin. In these areas we restore the density profile to its initial value and the velocities are gradually set to zero. The first sponge layer destroys the Kelvin front generated inside the strait and stops its propagation. It prevents this Kelvin front from disturbing the solution above the sill. The second sponge layer prevents the Kelvin wave front from propagating around the basin and perturbing the initial solution.

Several sensitivity experiments were run in order to investigate the basic physics of the problem. The different experiments are summarized in Table 1 •. Experiments E1, E2, and E3 were run with a linear version of the OPA7 model (the advection terms are suppressed in the momentum equation).

b. Flat bottom and sill (E1)

We first run an experiment (E1) with a flat bottom and sill in order to compare the model results with respect to the analytical developments.

The removal of the north–south gate generates a baroclinic Kelvin wave front propagating eastward along the southern shore (Fig. 5 •) as described by Gill (1976). The velocity of the front is 1.2 m s^{-1} in agreement with the theoretical value of 1.4 m s^{-1} . West of the strait, a baroclinic steady coastal current about 30 km wide appears behind the front.

The circulation reaches a quasi-stationary state after about 10 days of integration. Along the western coast of the strait a baroclinic current due to the propagation of Kelvin waves inside the strait is generated (Fig. 6 •). At the strait level, a large barotropic cyclonic gyre centered on the sill has developed (Fig. 7 •). Close to the sill, the flow is almost parallel to it. The zonal velocity has opposite signs on both sides of the sill. We also observe a vertical shear close to the sill due to the baroclinic component. At the surface and in the sill region the velocity is small and continuous, whereas in the deep layer there is a strong horizontal shear above the step (Fig. 8 •). Far away from the sill the flow is almost barotropic.

The time evolution of the zonal velocity above the sill (Fig. 9 •) shows that the vertical structure is mainly barotropic, with an amplitude increasing with time, before the arrival of a baroclinic component. This phenomenon is due to the fact that the barotropic double Kelvin waves have a higher phase speed than the baroclinic waves.

The numerical experiment is in good qualitative agreement with the analytical predictions. Indeed, the incident Kelvin front generates baroclinic and barotropic double Kelvin waves along the sill and a Kelvin front along the western coast of the strait. As deduced from the analytical calculations, the baroclinic double Kelvin waves only generate significant transport close to the sill (depending on the internal Rossby radius), while far away from the sill the velocity is induced by barotropic waves whose transversal scale is much larger than the baroclinic wave scale.

Let us now test the results quantitatively (Fig. 10 •). The barotropic transport in the gyre and the transport associated with the transmitted Kelvin front east of the strait computed by the numerical model are identical to the theoretical ones computed in section 2. The initial baroclinic transport [0.5 Sv ($\text{Sv} \equiv 10^6 \text{ m}^3 \text{ s}^{-1}$)] splits into two transports: one entering the strait (0.35 Sv) and the other transmitted across the strait and flowing along the east coast of the strait (0.08 Sv). The

sum of these last two baroclinic transports is not equal to the initial one, and the computed transports associated with the Kelvin front propagating into and across the strait are slightly weaker (by 20%) than the theoretical transports computed analytically (Fig. 11). This discrepancy may arise from the more complex response of the numerical model, which generates Poincaré waves; from the no-slip boundary condition at the coast; or from the diffusion of momentum, which is present in the numerical model.

The analytical study shows that the transports of the transmitted Kelvin front and of the Kelvin front inside the strait depend on the depth of the strait. Therefore, we tested this point with the model by reducing the total depth of the strait to 350 m. The transports associated with the transmitted front and the strait Kelvin front vary as predicted (the transport of the transmitted Kelvin front increases as the depth of the sill decreases), but with still an underestimation of the Kelvin front inside the strait. However, an extreme case can be encountered: when the strait depth is shallower than the thermocline, no flow is induced inside the strait and the incident Kelvin wave is transmitted with no amplitude change.

Another important parameter of this study is the width of the strait. In the present experiment we have modeled the Strait of Sicily by a rectangular channel 130 km wide. The real bathymetry of the strait is obviously more complicated since at 400 m the width of the strait is about 50 km. We therefore made another experiment with a narrower rectangular strait of width 50 km. The results are essentially the same, even if the different components are more difficult to observe, that is, a Kelvin wave along the western shore of the strait and another one at the east generated by a cyclonic gyre centered above the sill.

c. Abrupt shelf topography along the Algerian coast (experiment E2)

The bottom topography along the Algerian coast is not flat but presents a steep shelf, which may change the nature of the incident current by adding a barotropic component. This may modify the behavior of the current at the strait level, so we improved our representation of the bottom topography. We chose a topography of the form $H = H_0 - \Delta H e^{-y/r_H}$ in the main basin, where $H_0 = 1000$ m is the total depth at the coast ($y = 0$) and $\Delta H = 300$ m (Fig. 12). The offshore horizontal topography length scale r_H is equal to 50 km. The bottom is still flat inside the strait.

In a two-layer fluid with bottom topography and a rigid lid, different types of coastal trapped waves can be observed (Allen 1975), that is, an internal Kelvin wave and barotropic shelf waves, that are solutions of Eqs. (2.10), (2.12). These waves can be strongly coupled if the internal Rossby radius is close to a characteristic length for the topography H/H_y , which is not the case here (it would require $r_H \approx 5$ km).

1) RESULTS

We still observe a modified baroclinic Kelvin wave as in Wang (1974), but the presence of bottom topography also induces the propagation of topographic waves. These waves propagate eastward but with a phase velocity slower than the baroclinic Kelvin front. The Kelvin front arrives at the strait after five inertial periods, whereas the barotropic part of the incident flow arrives after ten inertial periods.

In the incident current, the barotropic flow approximately compensates the baroclinic component due to the Kelvin wave in the lower layer. The resulting current thus is concentrated in the surface layer with a weak westward current in the bottom layer (Fig. 13). This structure seems closer to the Mediterranean case (Herbaut et al. 1996) than the flat bottom case.

In the strait, a baroclinic Kelvin front is still generated along the western coast of the strait. The transport of the current induced by this front is the same as in the flat bottom case (Figs. 14 and 15). In the strait, the barotropic transport due to the propagation of the double Kelvin waves is also similar to the one obtained in the flat bottom case.

But east of the strait in the east–west basin, the circulation changes. Contrary to the flat bottom case, the current presents a barotropic component, that is, the flow is directed eastward on the whole depth (Fig. 16). Moreover, the current east of the strait presents a stronger barotropic component than the incident current (Fig. 17).

The transmitted baroclinic transport decreases when topography along the Algerian coast is present, whereas the barotropic transport is increased.

2) DISCUSSION

As in the lock exchange experiment made by Hsieh and Gill (1984), the initial density gradient generates a Kelvin front and shelf waves. In experiment E2, however, the Kelvin front propagates faster than the shelf waves. The Kelvin front

propagates the initial density gradient, which was located at the coast (at $x = -L$) up to the strait. In both cases (i.e., with flat bottom and with bottom topography), the density gradient was the same, and therefore the adjustment over the sill is the same at the arrival of the Kelvin front. According to Hsieh and Gill, each shelf wave mode propagates the projection of the forcing [$\nabla H \times \nabla(ap_0 + g'h)$] over the shelf wave eigenfunctions. These eigenfunctions, calculated in the basin, are equal to 0 at the coast where $y = 0$ (i.e., at the latitude of the strait). When these waves arrive at the longitude of the strait, they do not propagate any forcing at the entrance of the strait and therefore do not change the solution in the strait.

We note that the current east of the strait along the southern coast of the basin presents a barotropic component higher than that of the incident current. We offer the following explanation for this feature: The double Kelvin waves propagate a zonal surface pressure gradient perturbation (and also an interface perturbation). In the flat bottom case, when the double Kelvin waves arrive at the eastern corner of the strait, this surface pressure perturbation is totally compensated by an interface variation, and there is propagation of a baroclinic Kelvin front along the southern coast of the east–west basin. In the presence of bottom topography, the surface pressure gradient perturbation generates the propagation of topographic waves and therefore the barotropic component of the current is reinforced. The barotropic response is higher than in the western part of the east–west basin because the presence of the topographic gradient associated with the sill increases the forcing term [$\nabla H \times \nabla(ap_0 + g'h)$].

This experiment shows that the current flowing from the strait into the east–west basin turns right and follows the southern coast of the basin and also points out the importance of the bottom topography. This result can be compared with the observations of Astraldi (1995, personal communication), which suggest that the flow of Levantine Intermediate Water veers right when entering the Western Mediterranean Sea through the Strait of Sicily. However, this comparison should be made very carefully because, in the model, the stratification is only represented by a two-layer fluid and the characteristics of the LIW are not taken into account.

d. Large shelf topography (experiment E3)

As there is a large continental shelf off Tunisia, we added a simplified continental shelf on the west side of the basin. The continental shelf is represented by a flat domain 30 km wide and a depth of 250 m connected to a shelf slope 20 km wide (Fig. 18). Since the topography is located between $y = -a$ and $y = 0$, the shelf waves will interact with the strait and might modify the solution.

After 8 days, we observe a circulation similar to the flat bottom experiment, that is, the propagation of a Kelvin front inside the strait and of a double Kelvin front along the sill. The transport of the baroclinic Kelvin front propagating along the western coast of the strait and of the baroclinic Kelvin front propagating east of the strait are the same as the flat bottom experiment transports. However, the transition phase is different.

The initial density gradient still generates a baroclinic Kelvin front and shelf waves. In this case, however, the shelf wave phase velocity is faster than the Kelvin front phase velocity. When the shelf waves arrive at the sill, they generate a similar qualitative adjustment as in E1 along the sill (Fig. 19) and along the eastern part of the southern coast of the west–east basin, but the transport along the western coast of the strait is different from that of the steady state of E1. However, the arrival of the incident baroclinic Kelvin front reinforces this transport so that the final transport reaches a value identical to the one obtained in E1.

In E3, the initial density gradient crosses latitude $y = 0$ and extends south of this latitude. Therefore the shelf wave eigenfunctions are not equal to zero at $y = 0$. At point $(x = -L, y = 0)$, there is generation of vorticity due to the step discontinuity [$\nabla H \times \nabla(ap_0 + g'h)$]. This perturbation of vorticity, which is similar to that obtained in E1 at point $(x = 0, y = 0)$, is propagated by shelf waves up to the strait. Thus at point $(x = 0, y = 0)$, that is, at the longitude of the western side of the strait), since the forcing is similar to that found in E1, there is generation of a double Kelvin front over the sill. In the region $(x > 0, -a < y < 0)$ there is no more topography. Therefore, the perturbation of vorticity generated by the shelf topography and propagated by the shelf waves generates a baroclinic Kelvin front along the western coast of the strait. The initial density gradient at $x = -L$ also generates a baroclinic Kelvin front above the continental shelf. Arriving at the strait some time after the shelf waves, this baroclinic Kelvin front turns right and reinforces the current generated along the western coast of the strait. When the baroclinic Kelvin front has arrived, the initial alongshore pressure gradient associated to the density gradient located at $x = -L$ is propagated at $x = 0$. Since the forcing here is equal to the flat bottom case forcing, the solution is of the same magnitude.

4. Conclusions

The goal of this paper is to understand the circulation of the Strait of Sicily and more specifically the separation of the flow of Atlantic water and the path of the intermediate flow entering the Western Mediterranean Sea through the Strait of Sicily. We tested three different idealized topographic features that are important in the dynamics of the strait: the depth of

the sill (which is represented by a step topography), the presence of a bottom topography along the African coast, and the presence of a continental shelf along the Tunisian coast west of the strait. In these studies, the Atlantic incident current is generated by the propagation of a baroclinic Kelvin front and shelf waves when the topography is present. Therefore, we studied the interaction of this front with a strait, which is represented as the connection of a long deep east–west basin with a shallower north–south basin. Previous analytical studies in a similar domain were made by [Longuet-Higgins \(1968\)](#), [Pinsent \(1971\)](#), and [Gill et al. \(1986\)](#) but mostly in a barotropic case. They displayed the propagation of double Kelvin waves along the step discontinuity. In a simple analytical part, we therefore describe the double Kelvin waves generated in a two-layer fluid and propose a circulation scheme for the strait. At its arrival at the western corner of the strait, the incident baroclinic Kelvin front generates a southward propagation of a baroclinic Kelvin front inside the strait and a propagation of double Kelvin waves trapped along the sill. At the eastern corner of the strait, continuity of the transport induces the eastward propagation of a second baroclinic Kelvin front along the southern coast of the east–west basin. This mechanism explains the separation of the Atlantic current at the entrance of the Strait of Sicily. Indeed, at the western corner of the strait the surface flow divides into two branches. One branch enters the strait and follows the western coast of the strait. This flow is generated by the baroclinic Kelvin front, which propagates southward inside the strait. The second branch flows along the step discontinuity (the current being induced by the double Kelvin waves) and east of the strait along the southern coast of the east–west basin (the current being induced by the second baroclinic Kelvin front). In the second layer, the westward incident flow does not enter the strait as it is constrained by the coast, but follows the escarpment. This westward current is fed at the eastern corner of the strait by both a current flowing out of the strait and a westward current flowing along the southern coast of the east–west basin east of the strait (this current is generated by the Kelvin front, which propagates east of the strait). The transports of these currents depend on the ratio of the baroclinic Rossby radii; that is, they are a function of the height of the step: the shallower the sill, the smaller the transport of the surface current entering the strait at the western corner and the higher the current transmitted across the strait. If we apply the computation (3.21) at the Strait of Sicily ($H_1 = 150$ m, thickness of the Atlantic water layer; $H^- = 500$ m, depth of the strait; $H^+ = 3000$ m, mean depth of Tyrrhenian Sea), we find a transport in the strait 73% of the incident transport, which is close to the estimate of [Béthoux \(1980\)](#), who finds two-thirds of the incident transport.

The numerical experiments agree with the results of the analytical study for both the structure of the flow and the quantitative transport. Particularly, the sensitivity experiments with different conditions for the strait depth, width, or the surface-layer thickness give expected results. We also ran the same experiments with nonlinear terms included. The results are quasi-identical during the first 12 days. After this, the nonlinearity drives oscillations associated with baroclinic and barotropic instabilities and the physics of the interaction of the circulation with the strait is hardly tractable analytically. Furthermore, the density front at $x = -L$ is advected toward the strait as in [Hermann et al. \(1989\)](#) and directly interacts with the strait changing the conditions of the experiment.

The experiments with bottom or shelf topography show that the response inside the strait is not sensitive to topographic structures. In the experiment with bottom topography, the topographic waves do not “feel” the presence of the strait and they propagate eastward along the escarpment without influencing the response inside the strait. However, the presence of bottom topography modifies the vertical structure of the current, which flows along the southern coast of the basin east of the strait. The pressure gradient perturbation propagated by the double Kelvin waves to the east of the strait generates the propagation of topographic waves east of the strait. A barotropic component of the current therefore appears. This result can be interpreted as a confirmation of the observations of Astraldi (1995, personal communication) of a vein of LIW turning right at the exit of the strait. Moreover, as the shelf waves generated by the bottom topography do not enter the strait, the ratio of the transport entering the strait compared with the transport associated with the current east of the strait decreases. On the other hand, the shelf topography along the Algerian coast does not seem to play a major role in the circulation of the strait.

Due to the idealized character of the study, the problem presents some limitations. First, the flow of Atlantic water is modeled by a coastal current generated by the propagation of a baroclinic Kelvin front. In the real ocean the Atlantic inflow at the entrance of the strait is more eddylike rather than flowing as a well-defined coastal current. In this case, how does the topography of the strait influence these eddies?

Furthermore, the results of the above study can be easily extended to other oceanic situations. It could be used to interpret the path of surface current impinging on a continental shelf or the trajectory of deep flows, which are constrained by topography when they encounter deep trenches.

Acknowledgments

We would like to thank Dr. L. Mortier of ENSTA for fruitful discussions. We are grateful to P. Delecluse of LODYC for providing the 3D primitive equation model OPA. This work is a contribution to the SALTO and MTPII MATER projects supported by the AVICENNE and EC MAST programs, respectively.

REFERENCES

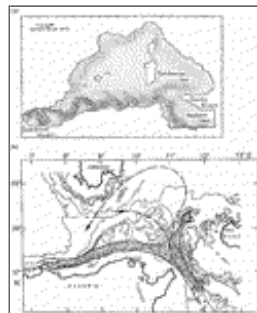
- Allen, J. S., 1975: Coastal trapped waves in a stratified ocean. *J. Phys. Oceanogr.*, **5**, 300–325..
- Andrich, P., P. Delecluse, C. Levy, and G. Madec, 1988: A multitasked ocean general circulation model of the ocean. *Proc. Fourth Int. Symp. on Science and Engineering on Cray Supercomputers*, Minneapolis, MN, Cray Research Inc., 407–428..
- Béthoux, J. P., 1980: Mean water fluxes across sections in the Mediterranean Sea, evaluated on the basis of water and salt budgets and of observed salinities. *Oceanol. Acta*, **3**, 79–88..
- Buchwald, V. T., 1968: The diffraction of Kelvin waves at a corner. *J. Fluid Mech.*, **31**, 193–205..
- Crépon, M., and C. Richez, 1982: Transient upwelling generated by two-dimensional atmospheric forcing and variability in the coastline. *J. Phys. Oceanogr.*, **12**, 1437–1457..
- Gill, A. E., 1976: Adjustment under gravity in a rotating channel. *J. Fluid Mech.*, **77**, 603–621..
- , M. K. Davey, E. R. Johnson, and P. F. Linden, 1986: Rossby adjustment over a step. *J. Mar. Res.*, **44**, 713–738..
- Herbaut, C., L. Mortier, and M. Crépon, 1996: A sensitivity study of the general circulation of the Western Mediterranean Sea. Part I: The response to density forcing through the straits. *J. Phys. Oceanogr.*, **26**, 65–84..
- Hermann, A. J., P. Rhines, and E. R. Johnson, 1989: Nonlinear Rossby adjustment in a channel beyond Kelvin waves. *J. Fluid Mech.*, **205**, 469–502..
- Hsieh, W. H., and A. E. Gill, 1984: The Rossby adjustment problem in a rotating stratified channel, with and without topography. *J. Phys. Oceanogr.*, **14**, 424–437..
- LeBlond, P. H., and L. A. Mysak, 1978: *Waves in the Ocean*. Elsevier, 602 pp..
- Longuet-Higgins, M. S., 1968: On the trapping of waves along a discontinuity in a rotating ocean. *J. Fluid Mech.*, **31**, 417–434..
- Manzella, G., G. P. Gasparini, and M. Astraldi, 1988: Water exchange between the eastern and western Mediterranean Sea through the Strait of Sicily. *Deep-Sea Res.*, **35**, 1021–1035..
- Madec G., M. Chartier, and M. Crepon, 1991a: Effect of thermohaline forcing variability on deep water formation in the Western Mediterranean Sea: A high resolution three dimensional numerical study. *Dyn. Atmos. Oceans*, **15**, 301–332..
- , —, P. Delecluse, and M. Crepon, 1991b: Numerical study of deep-water formation in the northwestern Mediterranean sea. *J. Phys. Oceanogr.*, **21**, 1349, 1371..
- Millot, C., 1987: Circulation in the Western Mediterranean Sea. *Oceanol. Acta*, **10**, 143–149..
- Pacanowski, R. C., and S. G. Philander, 1981: Parametrization of vertical mixing in numerical models of tropical oceans. *J. Phys. Oceanogr.*, **11**, 1443–1451..
- Pinsent, H. G., 1971: The effect of depth discontinuity on Kelvin wave diffraction. *J. Fluid Mech.*, **45**, 747–758..
- Speich, S., G. Madec, and M. Crepon 1996: A Strait outflow circulation process study: The case of the Alboran sea. *J. Phys. Oceanogr.*, **26**, 320–340..
- Wajsbowicz, R. C., 1991: On stratified flow over a ridge intersecting coastlines. *J. Phys. Oceanogr.*, **21**, 1407–1437..
- Wang, D. P., 1975: Coastal trapped waves in a baroclinic ocean. *J. Phys. Oceanogr.*, **5**, 326–333..
- Willmott, A. J., 1984: Forced double kelvin waves in a stratified ocean. *J. Mar. Res.*, **42**, 319–358..

Tables

Table 1. Synthetic description of the different numerical experiments.

--

Figures



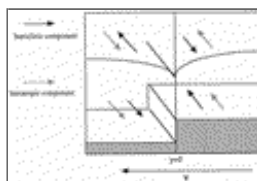
[Click on thumbnail for full-sized image.](#)

Fig. 1. (a) Surface velocity in the Western Mediterranean Sea computed by a primitive equation model with real topography forced by the inflow at the Strait of Gibraltar (from [Herbaut et al. 1996](#)). The separation of the Algerian Current into two branches at the level of the Strait of Sicily can be clearly seen. (b) Actual geometry and bottom topography of the strait with a schematization of the separation of the Algerian Current (shaded arrows). The dotted arrows represent the path of Levantine water.



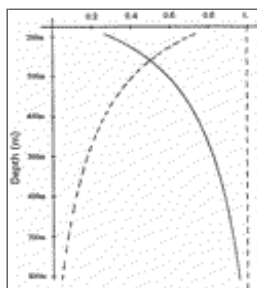
[Click on thumbnail for full-sized image.](#)

Fig. 2. Geometry of the studied domain: (a) plan view showing the main basin, the strait, and the two sponge layers. The east–west length is 650 km and the north–south length is 400 km. (b) Vertical meridional section of the basin at the level of the strait along the dotted line in [Fig. 2a](#) in case of a flat bottom topography.



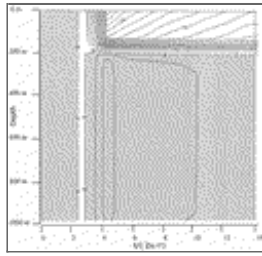
[Click on thumbnail for full-sized image.](#)

Fig. 3. Schematic figure of a long double Kelvin wave at the sill. The hatched arrows represent the barotropic velocity; the solid arrows represent the baroclinic velocity. The velocities are in opposite directions on the two sides of the sill. The baroclinic velocities are in the same direction as the barotropic velocities in the bottom layer and in opposite direction in the surface layer.



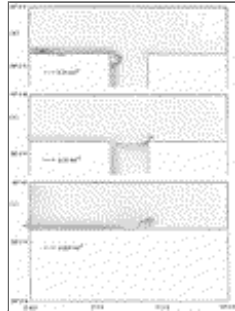
[Click on thumbnail for full-sized image.](#)

Fig. 4. Analytical solution: baroclinic transport in the strait (full line) and transmitted across the strait (dotted line) vs the incident baroclinic transport as a function of the depth of the sill (the depth of the basin is 1000 m).



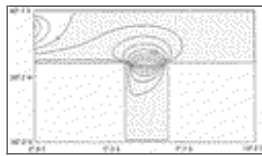
[Click on thumbnail for full-sized image.](#)

Fig. 5. Time evolution of the vertical profile of the zonal velocity just west of the strait in experiment E1. The horizontal axis corresponds to a nondimensional time $t' = t/(2\pi/f)$, where f is the Coriolis parameter, and the vertical axis is the depth from the surface to the bottom. The unit for velocity is in millimeters per second. Shaded areas correspond to westward velocities. During the first three inertial periods, the velocity in the surface layer is nearly equal to zero corresponding to the travel time of the Kelvin wave to reach the strait.



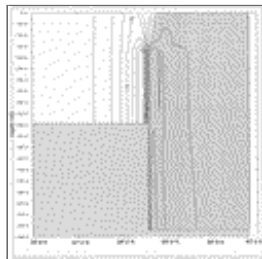
[Click on thumbnail for full-sized image.](#)

Fig. 6. Plan view of the velocity field at 10 days in experiment E1: (a) at surface, maximum velocity 0.34 m s^{-1} ; (b) at 240 m, maximum velocity 0.10 m s^{-1} ; (c) at 600 m, maximum velocity 0.035 m s^{-1} .



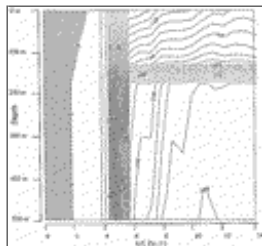
[Click on thumbnail for full-sized image.](#)

Fig. 7. Plan view of the barotropic streamfunction in experiment E1. The interval contour is equal to $80 \times 10^{-3} \text{ Sv}$.



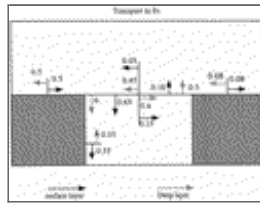
[Click on thumbnail for full-sized image.](#)

Fig. 8. Meridional vertical section of zonal velocities across the middle of the sill in experiment E1. The contour interval for velocity is 0.03 m s^{-1} . Shaded areas correspond to westward velocities.



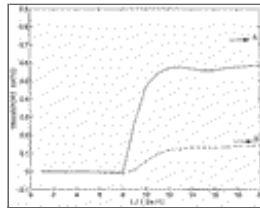
[Click on thumbnail for full-sized image.](#)

Fig. 9. Time evolution of the vertical profile of the zonal velocity in the open sea close to the middle of the strait (experiment E1). The horizontal axis corresponds to a nondimensional time $t' = t/(2\pi/f)$, where f is the Coriolis parameter, and the vertical axis is the depth from the surface to the bottom. The contour interval for velocity is 0.01 m s^{-1} . Shaded areas correspond to westward velocities.



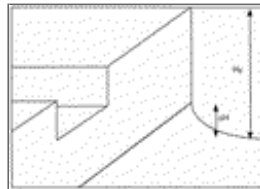
[Click on thumbnail for full-sized image.](#)

Fig. 10. Experiment E1. Scheme of the transports in each layer (in Sv): black arrows represent the transport in the surface layer; dotted arrows represent the transport in the second layer. The numbers are in Sv. The initial baroclinic transport (0.5 Sv) splits into transports: one entering the strait (0.35 Sv) and the other transmitted across the strait, flowing along the east coast of the strait (0.08 Sv).



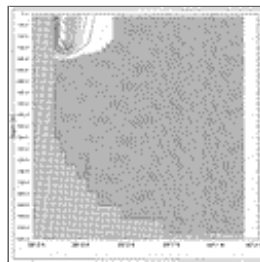
[Click on thumbnail for full-sized image.](#)

Fig. 11. Experiment E1. Ratio of the model transport associated with the baroclinic Kelvin front along the west coast of the strait vs the incident transport (plain line) and the theoretical ratio (A-arrow). Ratio of the model baroclinic transport in the current east of the strait vs the incident transport (dashed line) and the theoretical ratio (B-arrow).



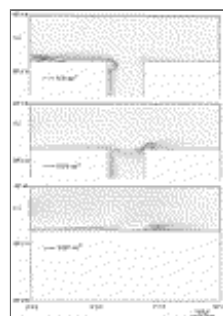
[Click on thumbnail for full-sized image.](#)

Fig. 12. Geometry of the domain in the experiment with bottom topography (expt E2).



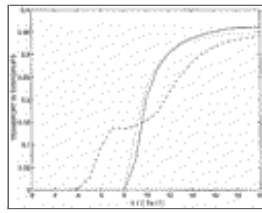
[Click on thumbnail for full-sized image.](#)

Fig. 13. Experiment E2. Meridional vertical section of the zonal incident velocity west of the strait at 15 days. Shaded areas correspond to westward velocities.



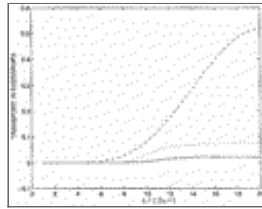
[Click on thumbnail for full-sized image.](#)

Fig. 14. Plan view of the velocity field at 15 days in experiment E2: (a) at surface, maximum velocity 0.36 m s^{-1} ; (b) at 240 m, maximum velocity 0.078 m s^{-1} ; (c) at 600 m, maximum velocity 0.037 m s^{-1} .



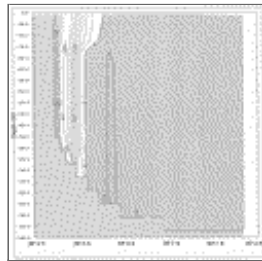
[Click on thumbnail for full-sized image.](#)

Fig. 15. Time evolution of the transport associated with the baroclinic Kelvin front inside the strait: (solid) in experiment E1, (dashed) in experiment E2, and (dotted) in experiment E3. The incident transport is close to 0.5 Sv in the three experiments.



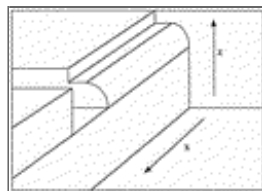
[Click on thumbnail for full-sized image.](#)

Fig. 16. Time evolution of the transport east of the strait (transmitted transport across the strait) for (dashed) barotropic transport in the experiment E2, (solid) baroclinic transport in the experiment E2, and (dotted) baroclinic transport in the experiment E1.



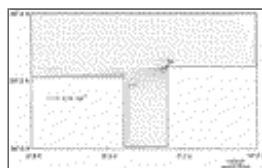
[Click on thumbnail for full-sized image.](#)

Fig. 17. Experiment E2. Meridional vertical section of the zonal velocity east of the strait at 15 days. Shaded areas correspond to westward velocities. The transmitted velocity is mainly barotropic in opposition to the incident current west of the strait, which is mainly baroclinic as shown in [Fig. 13](#).



[Click on thumbnail for full-sized image.](#)

Fig. 18. Geometry of the domain in the experiment with a shelf topography.



[Click on thumbnail for full-sized image.](#)

Fig. 19. Experiment E3. Velocity field at 240 m after 6 days before the arrival of the incident baroclinic Kelvin wave. The fluid flows eastward, whereas the flow is westward in E1 after the arrival of the incident baroclinic Kelvin wave ([Fig. 6](#)). This velocity is linked to the shelf waves, which propagate faster than the baroclinic Kelvin waves. The velocity maximum is 0.10 m s^{-1} .

Corresponding author address: Dr. Michel Crépon, LODYC, Université Pierre et Marie Curie, Tour 14-2e stage-4 Place Jussieu, 75252 Paris, Cedex 05, France.

E-mail: mc@lodyc.jussieu.fr

[top ▲](#)



© 2008 American Meteorological Society [Privacy Policy and Disclaimer](#)

Headquarters: 45 Beacon Street Boston, MA 02108-3693

DC Office: 1120 G Street, NW, Suite 800 Washington DC, 20005-3826

amsinfo@ametsoc.org Phone: 617-227-2425 Fax: 617-742-8718

[Allen Press, Inc.](#) assists in the online publication of *AMS* journals.